Journal of Alloys and Compounds 678 (2016) 297–303

Contents lists available at ScienceDirect

Journal of Alloys and Compounds

journal homepage: http://www.elsevier.com/locate/jalcom

Hydrogen storage properties of a destabilized MgH_2–Sn system with TiF_3 addition

M. Ismail [a, *], F.A. Halim Yap [a], N.N. Sulaiman [a], M.H.I. Ishak [b]

[a] School of Ocean Engineering, Universiti Malaysia Terengganu, Terengganu, Malaysia
[b] Control and Mechatronics Department, Faculty of Electrical Engineering, Universiti Teknologi Malaysia, 81310, Skudai, Johor, Malaysia

ARTICLE INFO

Article history:
Received 5 October 2015
Received in revised form
20 March 2016
Accepted 22 March 2016
Available online 23 March 2016

Keywords:
Energy storage materials
Metal hydride
Magnesium hydride
Catalytic effect

ABSTRACT

The MgH_2–Sn system is considered a promising reactive metal composite for hydrogen storage. Several ratios of MgH_2–Sn (2:1, 3:1 and 4:1) destabilized system were investigated experimentally using a ball milling method. Based on the temperature-programme desorption results, the onset dehydrogenation temperature of the MgH_2–Sn composite was consisted of two steps in the range of 235–250 °C and 325–340 °C. TiF_3 catalyst was introduced to enhance the desorption temperature of the MgH_2–Sn (4:1) system. The onset dehydrogenation temperature of the $4MgH_2$–Sn-10 wt% TiF_3 composite was reduced to approximately 100 °C and 205 °C compared to the MgH_2–Sn (4:1) and the as-milled MgH_2. The Kissinger analysis established that the apparent activation energy for the first stage of the $4MgH_2$–Sn composite was reduced from 149.0 kJ/mol to 114.0 kJ/mol after adding 10 wt% TiF_3. However, the addition of TiF_3 did not result in improvement of the absorption process. The improvement of the dehydrogenation properties of the MgH_2–Sn composite with the addition of TiF_3 was due to the formation of Ti-containing and F-containing species. These species played a catalytic role in improving the dehydrogenation properties of the MgH_2–Sn system.

1. Introduction

Hydrogen is one of the most valuable energy carriers in view of the current demand for pollution-free energy systems. One of the keys to effective hydrogen storage is to store enough hydrogen for automobile on-board applications. The current research and development of high capacity hydrogen storage materials are drawing intensive attention among investigators in the energy material field [1]. As an energy carrier, hydrogen is a proximate ideal because it can be generated from a diverse number of feedstocks and can be converted to the desired form of energy without releasing harmful emissions at the point source, thus reducing greenhouse gas emissions, criteria pollutants and dependence on fossil fuels [2]. Hydrogen can be stored in several forms: as a compressed gas, cryogenic liquid and solid-state. Hydrogen storage in solid-state form has been extensively studied compared to compressed gas and cryogenic liquid forms. Several classes of solid-state hydrogen storage materials have been developed, such as metal hydrides [3], complex hydrides [4–7] and carbon nanomaterials [8,9]. Metal hydrides have largely been investigated due to their benefits. Among the metal hydrides, the Mg-based hydride, MgH_2, meets many of the technological demands, such as large gravimetric hydrogen density (7.6 wt% H_2), abundant resources, low cost and good reversibility [10,11], but its sluggish kinetics of hydrogen sorption and high thermodynamic stability have delayed commercial application of this material. Intensive efforts have been devoted to overcome these barriers, such as the use of ball milling [12,13], adding catalysts [14–20] and combining with metal or other hydrides [21–27], to enhance the MgH_2 hydrogen sorption properties.

The combination of MgH_2 with other metals, also known as the destabilization concept has attracted the attention of many researchers with several studies conducted for the MgH_2–Sn system [28–31]. Based on the results of a study by Imamura et al. [30,31], it was found that the addition of Sn as a destabilizing agent to form the MgH_2–Sn composite significantly improved its hydrogen sorption properties. Even though the desorption temperature of the MgH_2–Sn system was reduced, it still did not meet the desired requirement for practical applications. Therefore, in order to improve the desorption temperature, a catalyst was introduced to the MgH_2–Sn system. There are no studies on the effect of the

* Corresponding author.
E-mail address: mohammadismail@umt.edu.my (M. Ismail).

http://dx.doi.org/10.1016/j.jallcom.2016.03.168
0925-8388/

catalyst on the storage properties of the MgH_2–Sn system. Therefore, it is an important issue for future research to discover any catalyst or additives that can improve the hydrogen storage properties of the MgH_2–Sn system. To the best of the authors' knowledge, no study has been conducted to classify the effect of TiF_3 as an additive on the hydrogen storage properties of MgH_2–Sn. Recently, Ismail et al. [32] stated that the formation of Ti-containing and F-containing active species plays a catalytic role in the MgH_2–⊜ $NaAlH_4$–TiF_3 system, which may promote the interaction of $NaAlH_4$ and MgH_2, and thus enhance the dehydrogenation of the MgH_2–$NaAlH_4$ system. The effect of TiF_3 on the dehydrogenation properties of MgH_2 was investigated by Ma et al. [33] who suggested that TiH_2 and MgF_2, formed in situ, played an important role in the enhancement of the dehydrogenation properties of MgH_2. Therefore, the present study hypothesised that the hydrogen storage properties of MgH_2–Sn could be improved by doping using the TiF_3 additive.

In this article, the addition of TiF_3 to improve the hydrogen storage properties of the MgH_2–Sn composite by ball milling was investigated for the first time. The hydrogen sorption properties of the MgH_2–Sn composite in the presence of TiF_3 were investigated by Sievert-type pressure-composition-temperature (PCT) apparatus and differential scanning calorimetry (DSC). To determine the particle's size and to clarify the reaction mechanism of the composite during the de/rehydrogenation process, scanning electron microscopy (SEM) and X-ray diffraction (XRD) were used, respectively. Next, the possible mechanism from the catalytic effect of TiF_3 in the MgH_2–Sn composite was discussed.

2. Experimental details

The initial materials, MgH_2 (hydrogen storage grade with 98% purity), Sn and TiF_3 were purchased from Sigma Aldrich and were used directly without any further purification. The milling experiments were performed in a planetary ball mill (NQM-0.4) by milling for 15 min, resting for 2 min and milling for another 15 min. This process was conducted in three cycles in a different direction at a rotation speed of 400 rpm using hardened stainless steel milling tools. The molar ratios of MgH_2 and Sn in this study were 2:1, 3:1 and 4:1. These composites are referred to as $2MgH_2$–Sn, $3MgH_2$–Sn and $4MgH_2$–Sn for simplicity. TiF_3 (10 wt%) was mixed with $4MgH_2$–Sn under the same conditions to investigate the catalytic effects. Pure MgH_2 was also prepared under the same conditions for comparison purposes. All handling of the powders, including weighing and loading, was performed in an argon atmosphere MBraun Unilab glove box.

For the temperature-programmed-desorption (TPD) and the sorption measurements, the sample was loaded into a sample vessel and sealed inside a glove box. The experiments were performed in a Sieverts-type pressure-composition-temperature (PCT) apparatus (Advanced Materials Corporation). This system covers the temperature range from room temperature to 500 °C at hydrogen pressures up to 10 MPa. The heating rate for the TPD measurement was 5 °C/min, and samples were heated in a vacuum chamber from room temperature to 450 °C.

Differential scanning calorimetry (DSC) analysis of the dehydrogenation process was performed on a Mettler Toledo thermogravimetric analysis/differential scanning calorimeter (TGA/DSC) 1. The sample was loaded into an alumina crucible in the glove box. The crucible was then placed in a sealed glass bottle to prevent oxidation during transportation from the glove box to the DSC apparatus. An empty alumina crucible was used as the reference. The samples were heated from room temperature to 500 °C under an argon flow of 30 ml/min, and different heating rates were used.

The samples for scanning electron microscopy (SEM) and X-ray diffraction (XRD) were also prepared in the glove box. The SEM samples were placed on carbon tape and coated with gold spray under a vacuum. The morphology of the samples was characterized using a scanning electron microscope (SEM; JEOL JSM-6360LA). In addition, the samples before and after desorption, as well as after the rehydrogenation stage, were characterized by a Rigaku Mini-Flex X-ray diffractometer with Cu Ka radiation. The patterns were scanned over diffraction angles from 20° to 80° with a speed of 2.00°/min. To avoid exposure to air during the measurement, the sample was spread uniformly on the sample holder and covered with plastic wrap.

3. Results and discussion

3.1. Dehydrogenation temperature

Fig. 1 shows the TPD (temperature-programmed desorption) results for the as-received MgH_2, the as-milled MgH_2 and the MgH_2 with Sn added (2:1, 3:1 and 4:1 M ratios). The as-received MgH_2 started to release hydrogen at approximately 434 °C and desorbed approximately 7.5 wt% hydrogen (7.6 wt% H_2 was theoretically released). After milling, the onset desorption temperature of the MgH_2 was reduced to approximately 355 °C, indicating that the milling process also influenced the onset decomposition temperature of the MgH_2. The ball milling technique is an effective way to activate magnesium or form composites for hydrogen storage [34] and influences the onset desorption temperature of MgH_2, as claimed by Huot et al. [12]. The as-milled MgH_2 released approximately 7.4 wt% hydrogen after 420 °C. After combining with Sn, there are two stages of dehydrogenation during the heating process. The first stage occurs within the temperature range from 235 to 250 °C, and the second dehydrogenation stage starts at approximately 325–340 °C and is completed at 380 °C. The first step at low temperature is due to the reaction of MgH_2 with Sn to irreversibly form the Mg_2Sn intermetallic compound (Reaction (1)), and the second step at relatively high temperature is due to hydrogen desorption from the remaining MgH_2 (Reaction (2)). This process is already known from the previously reported properties of the MgH_2–Sn system [30,31]. The onset decomposition temperature of the MgH_2 decreased dramatically after combining with Sn and was 100 °C and 164 °C lower than for the as-milled and as-received MgH_2, respectively. The total amount of hydrogen released

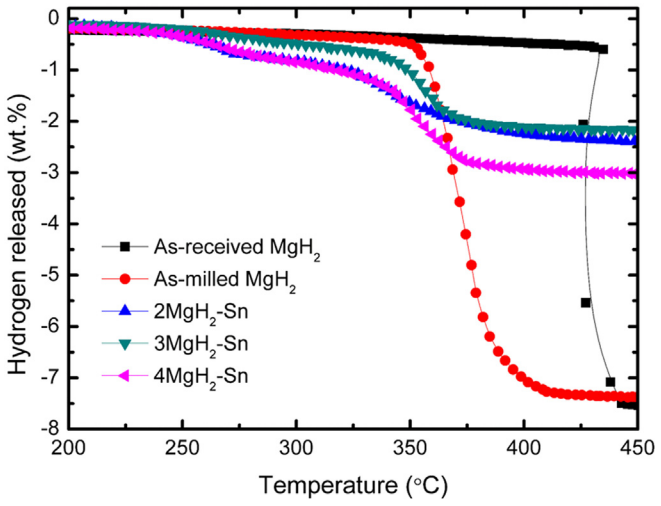

Fig. 1. TPD patterns for the dehydrogenation of the as-received MgH_2, as-milled MgH_2 and the MgH_2–Sn mixture with ratios of 2:1, 3:1, and 4:1.

was approximately 2.17 and 2.40 wt% for the 2:1 and 3:1 M ratio samples and 3.04 wt% for the 4:1 M ratio sample, which roughly agreed with the hydrogen content (about 2.34 wt%) calculated from the constituent composition of MgH_2 and Sn (Reaction (1)). In addition, the reduction of hydrogen capacity in the MgH_2/Sn samples (not exceeding 3.04 wt%) is due to the relatively high Sn addition level.

$$2MgH_2 + Sn \rightarrow Mg_2Sn + 2H_2 \quad (1)$$

$$MgH_2 \rightarrow Mg + H_2 \quad (2)$$

Fig. 2 presents the TPD curves for the dehydrogenation of the as-milled $4MgH_2$–Sn-10 wt% TiF_3 composite. The $4MgH_2$–Sn composite is also included for comparison. Upon addition of 10 wt% of TiF_3 to the $4MgH_2$–Sn, the onset dehydrogenation temperature of hydrogen decreased sharply. The TiF_3-doped $4MgH_2$–Sn composite sample starts to release hydrogen at 150 °C and 250 °C for the first and second stage, respectively, which represents respective reductions of 100 °C and 80 °C compared with $4MgH_2$–Sn. The two stages of dehydrogenation occurred during the heating process with a total liberation amount of 2.6 wt% H_2. The first stage proceeded within a temperature range of 140 °C to 160 °C and released approximately 1.5 wt% H_2, and the second stage started at 250 °C and was completed at 300 °C and released 1.1 wt% H_2. This result shows that the dehydrogenation temperatures for both stages in the $4MgH_2$–Sn composite were reduced significantly after the addition of TiF_3.

3.2. Differential scanning calorimetry

The DSC curves shown in Fig. 3 are for the $4MgH_2$–Sn and $4MgH_2$–Sn- 10 wt% TiF_3 composite. The plot for the $4MgH_2$–Sn composite shows characteristic peaks, specifically, an endothermic peak at 250 °C and 445 °C. The two endothermic DSC peaks are due to a dehydriding process, which is in accordance with that reported by Imamura et al. [30,31] and agrees well with the results observed in the TPD measurement in Fig. 1. Compared with the DSC plot of the $4MgH_2$–Sn composite, the characteristic peaks of the $4MgH_2$–Sn-10 wt% TiF_3 composite show two endothermic peaks at 230 °C and 360 °C. From the DSC results, it can be observed that the onset decomposition temperature was slightly higher than that of the TPD results in Fig. 2. This result is due to the different conditions

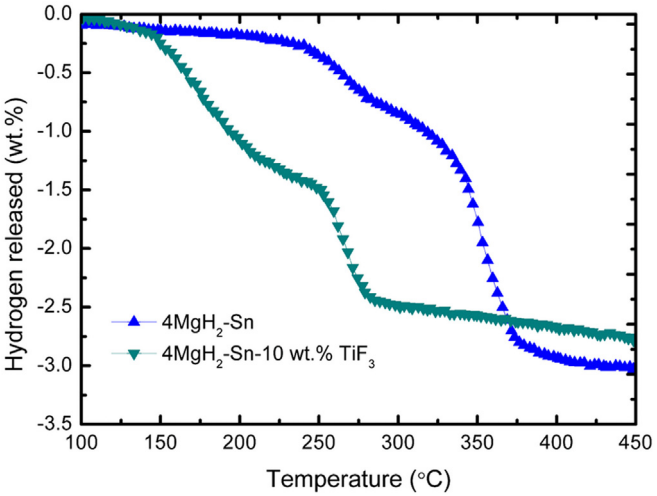

Fig. 2. TPD curves of the MgH_2–Sn system with and without TiF_3 doping.

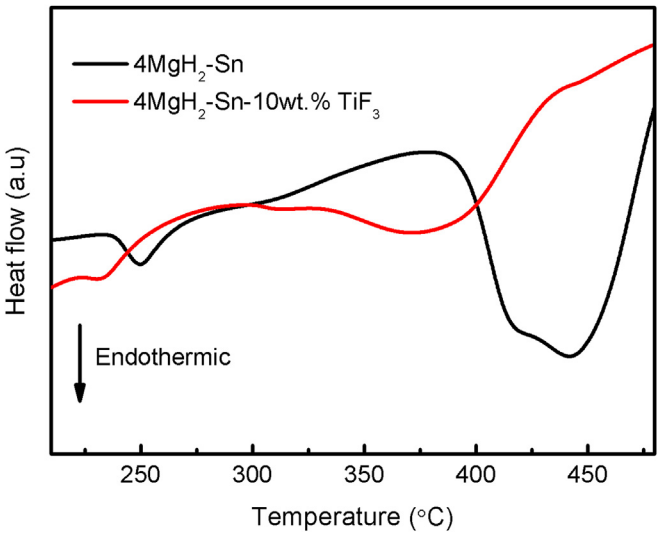

Fig. 3. DSC curves of $4MgH_2$–Sn and $4MgH_2$–Sn-10 wt% TiF_3 samples at a heating rate of 30 °C/min.

of the dehydrogenation measurement conducted in these two cases. The DSC measurement was run under 1 atm argon flow with a heating rate of 30 °C/min, whereas the TPD measurement was conducted from a 0.1 atm vacuum with a 5 °C/min heating rate, which generated the different driving forces during the desorption process, as discussed in our previous papers [35–38]. The Kissinger equation [39] was used to calculate the activation energy for the first stage of hydrogen released from the $4MgH_2$–Sn and $4MgH_2$–Sn-10 wt% TiF_3 composites. From the Kissinger equation, it can be observed that

$$\ln [\beta/T_p^2] = -E_A/RT_p + A \quad (3)$$

where β is the heating rate, T_p is the peak temperature in the DSC curve, R is the gas constant, and A is a linear constant. Thus, the activation energy, E_A, can be obtained from the slope in a plot of ln $[\beta/T_p^2]$ versus $1000/T_p$. Figs. 4 and 5 show the DSC traces for the $4MgH_2$–Sn and $4MgH_2$–Sn-10 wt% TiF_3 composites at different

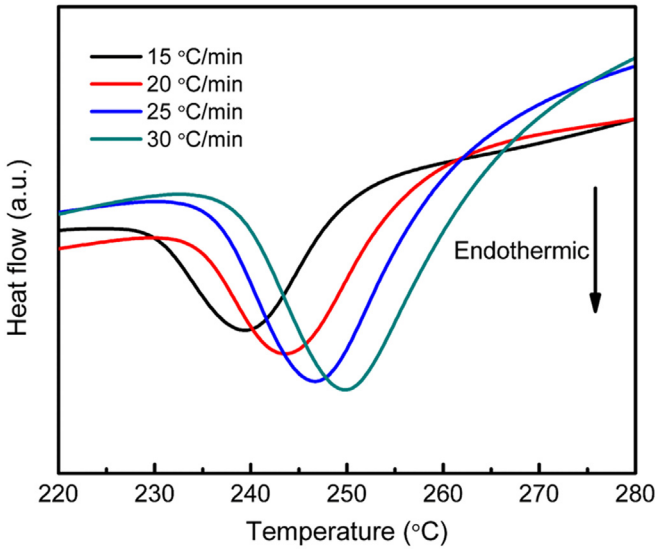

Fig. 4. DSC traces of the $4MgH_2$–Sn composite at different heating rates.

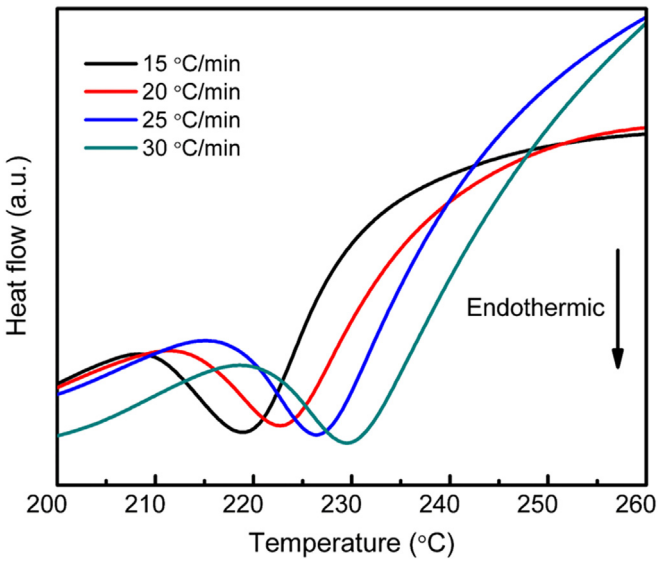

Fig. 5. DSC traces of the $4MgH_2$–Sn–TiF_3 composite at different heating rates.

heating rates. The apparent activation energy for the decomposition of the first stage of the $4MgH_2$–Sn composite is 149.0 kJ/mol, as shown in the Kissinger plot in Fig. 6. Meanwhile, from the same figure, it can be observed that the apparent activation energy of the first stage for the $4MgH_2$–Sn-10 wt% TiF_3 composite was reduced to 114.0 kJ/mol. This reduction suggests that the activation energy for the decomposition of $4MgH_2$–Sn was reduced after being mixed with TiF_3, which indicates that the TiF_3 additive plays an important role in reducing the activation energy of the $4MgH_2$–Sn composite.

3.3. Scanning electron microscopy

The SEM images of the as-received MgH_2 and the as-milled MgH_2, $4MgH_2$–Sn and $4MgH_2$–Sn-10 wt% TiF_3 are shown in Fig. 7. Based on the images, the as-milled MgH_2 (Fig. 7 (b)) has smaller sized particles compared to the as-received MgH_2 (Fig. 7 (a)). The particle size of the MgH_2 before milling was larger than 100 mm and had an angular shape. In addition, after ball milling the

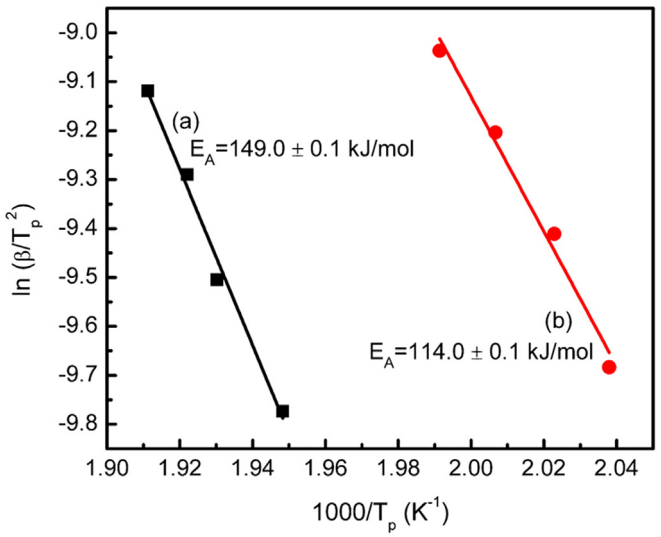

Fig. 6. Kissinger's analysis of $4MgH_2$–Sn (a) and $4MgH_2$–Sn-10 wt% TiF_3 (b).

MgH_2 with transition metal Sn, the size of the particles decreased significantly, as shown in Fig. 7 (c). Meanwhile, the addition of 10 wt% of TiF_3 to the $4MgH_2$–Sn (Fig. 7 (d)) resulted in smaller sized particles than the $4MgH_2$–Sn composites. The $4MgH_2$–Sn composite particles were broken into smaller sizes after the addition of TiF_3 additive due to the hardness of the additive. This phenomenon is similar to our previous report on K_2TiF_6 and K_2ZrF_6 doped MgH_2 [40,41], in which the hardness of the additive helped to break the MgH_2 particles into smaller sizes. Smaller particle sizes are found to increase the hydrogen sorption properties by two factors: a decrease of the diffusion length of hydrogen within the particles and an increase of the specific surface area and consequently an increase of the kinetic rates of all related surface reactions [42].

3.4. X-ray diffraction

To describe the mechanism for each stage in the dehydrogenation of the $4MgH_2$–Sn composite with and without TiF_3, XRD was applied, as shown in Fig. 8. After 1 h of milling, the MgH_2 (crystallizes in tetragonal space group *P42/mnm* with the lattice parameters a = 4.51680 Å and c = 3.02050 Å, as identified using the standard data JCPDS 74-934) and Sn (crystallizes in tetragonal space group *I41/amd* with the lattice parameters a = 5.83320 Å and c = 3.18200 Å, as identified using the standard data JCPDS 65-296) phases were detected in the as-milled $4MgH_2$–Sn composite (Fig. 8(a)). The dehydrogenation product after the first stage of dehydrogenation up to 320 °C is shown in Fig. 8(b). Clearly, Mg_2Sn (crystallizes in cubic space group *Fm3m* with the lattice parameter a = 6.765 Å, as identified using the standard data JCPDS 2-1087) peaks were present due to the reaction between MgH_2 and Sn, as shown in Reaction (1). Small amounts of MgH_2 and Sn peaks were also present at this stage. After further dehydrogenation up to 450 °C, only the Mg_2Sn peaks could be observed (Fig. 8(c)), and no Mg peaks were detected. The absence of Mg peaks is due to transformation into an amorphous state during the dehydrogenation process in the second stage. This phenomenon is similar to that for the Sn/MgH_2 composite, as reported by Imamura et al. [30,31]. In their report, after TPD measurements of Sn/MgH_2, the dehydrided sample showed the formation of Mg_2Sn with cubic structure and no peaks for Mg in the XRD. They also reported that in the TG measurements, Sn/MgH_2 showed TG traces consisting of two distinct steps of weight changes: the first desorption of hydrogen began from 187 °C with a weight loss of 2.0 wt%, followed by an additional loss of 1.4 wt% at 297 °C.

The XRD of the samples was acquired after ball milling of $4MgH_2$ and Sn with 10 wt% of TiF_3 for 1 h and after dehydrogenation process at 230 °C and at 450 °C, as shown in Fig. 9. From the graph, there were no additional diffraction peaks that suggested new phases or products resulting from the ball milling of $4MgH_2$–Sn and TiF_3. The peaks of MgH_2 and Sn can be observed in Fig. 9(a). The absence of the TiF_3 peaks is due to its transformation into an amorphous state during the 1 h of ball milling or the amount of TiF_3 being too little to be detected by the matrix of the XRD. This result is in accordance with our previous paper [32,43]. In Fig. 9(b), the XRD patterns were the same as in Fig. 9(a), which suggested that the active species peaks cannot be observed due to the amorphous state. In our previous paper [32], no phase containing F was detected before or after rehydrogenation, but the peak of Ti-containing alloy (Al–Ti alloy) was detectable in the MgH_2–⊜ $NaAlH_4$ matrix by XRD. For comparison, a new phase of LiF was identified after dehydrogenation and rehydrogenation process for the MgH_2–$LiAlH_4$–TiF_3 composite system. However, no phase containing Ti was detected due to the low concentration or amorphous phase, as reported by Mao et al. [43]. The pattern of the dehydrogenation process at 450 °C (Fig. 9(c)) presented major

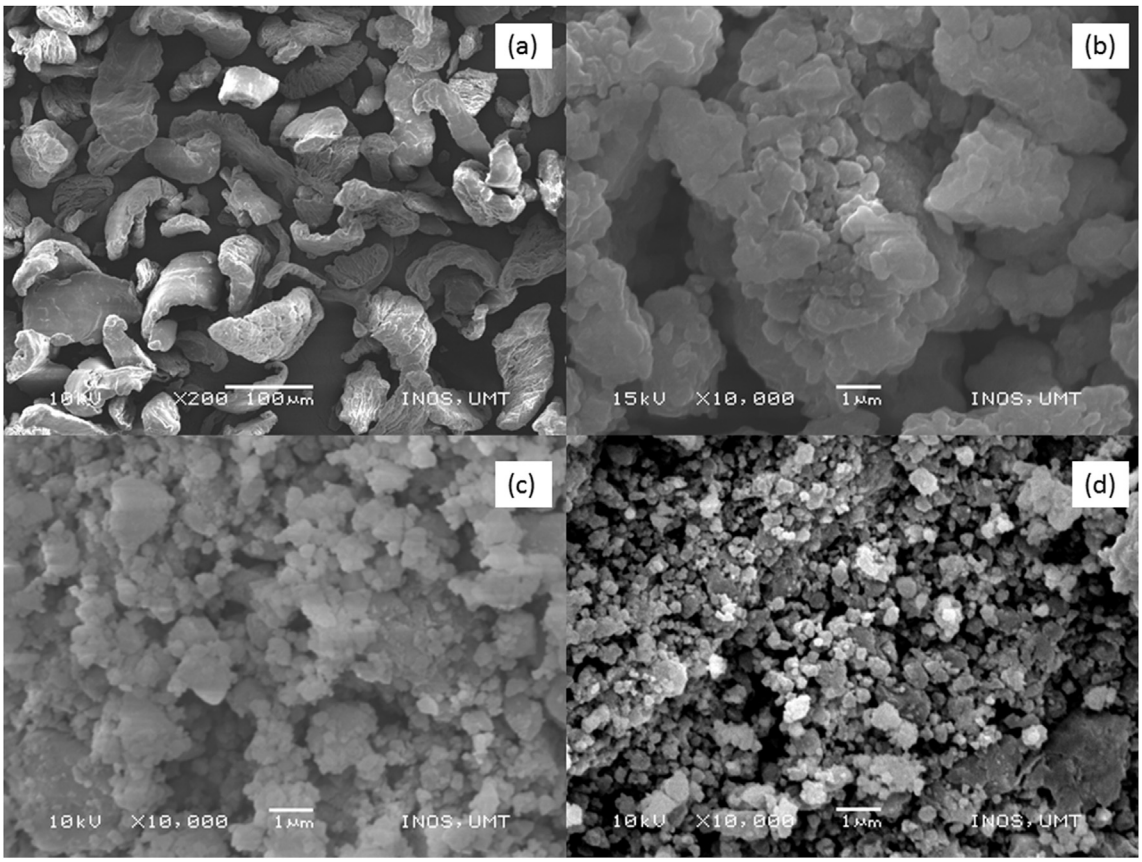

Fig. 7. SEM images of the as-received MgH_2 (a), as-milled MgH_2 (b), MgH_2–Sn (c), and MgH_2–Sn-10 wt% TiF_3 (d).

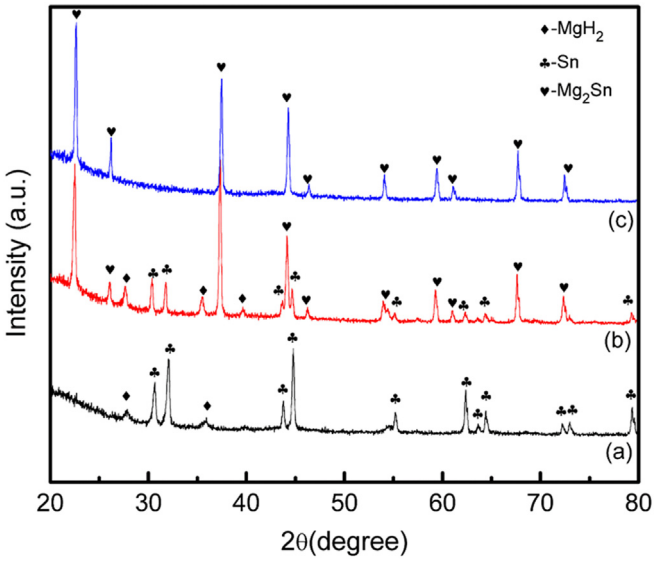

Fig. 8. XRD patterns of the $4MgH_2$–Sn composite after ball milling for 1 h (a), and after dehydrogenation at 320 °C (b) and at 450 °C (c).

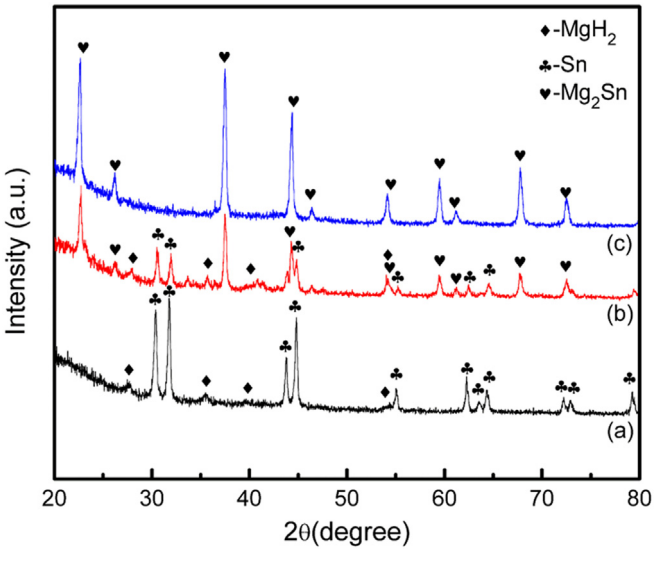

Fig. 9. XRD patterns of the $4MgH_2$–Sn-10 wt% TiF_3 composite after ball milling for 1 h (a) and after dehydrogenation at 230 °C (b) and at 450 °C (c).

peaks of Mg_2Sn.

To investigate the TiF_3-containing phase after ball milling and after dehydrogenation in more detail, we prepared a $4MgH_2$–Sn sample with 50 wt% TiF_3 because it is not easy to analyse the phase composition of the sample with 10 wt% TiF_3 by XRD. After increasing the amount of TiF_3 to 50 wt%, MgH_2 and Sn phases were detected along with some peaks of TiF_3 (crystallizes in rhombohedral space group *R-3c* with the lattice parameters a = 5.51900 Å, as identified using the standard data JCPDS 85-478), after 1 h ball milling, as shown in Fig. 10(a). The appearance of TiF_3 peaks in the XRD pattern indicated that increasing amount of the catalyst to 50 wt% was sufficient compared with 10 wt% of TiF_3. This

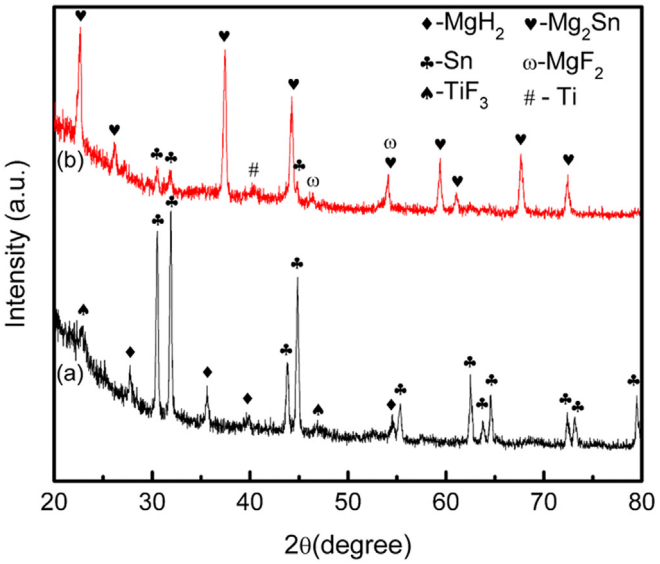

Fig. 10. XRD patterns of the $4MgH_2$–Sn-50 wt% TiF_3 composite after ball milling for 1 h (a) and after dehydrogenation at 450 °C (b).

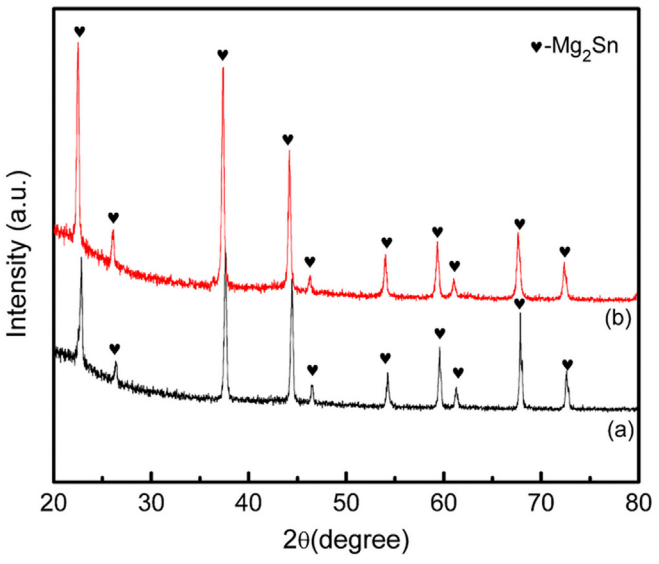

Fig. 11. XRD patterns after the rehydrogenation process at 300 °C of the $4MgH_2$–Sn composite (a) and $4MgH_2$–Sn–TiF_3 composite (b).

phenomenon is similar to that for MgH_2-50 wt% K_2TiF_6 that was ball milled for 1 h, as reported in our previous paper [40]. After dehydrogenation, compared with the dehydrogenated $4MgH_2$–Sn-10 wt% TiF_3 sample (Fig. 9(c)), new diffraction peaks were formed, which were MgF_2 (crystallizes in cubic space group *Pa-3* with the lattice parameter a = 4.792 Å, as identified using the standard data JCPDS 38-882) and Ti (crystallizes in hexagonal space group *P63/mmc* with the lattice parameters a = 2.92 Å and c = 4.67 Å, as identified using the standard data JCPDS 1-1198), as shown in Fig. 10(b). The formation of Ti species after dehydrogenated is due to the fact that the Ti containing phase does not fully react with hydrogen to form the TiH_2 species [40]. From the XRD pattern for the dehydrogenated samples, the F-containing species MgF_2 was detected due to their higher concentration after increasing the amount of additive to 50 wt% compared with the $4MgH_2$–Sn-10 wt % TiF_3 (Fig. 9(c)) sample with no detection of F species. There were Sn peaks after the dehydrogenation process, indicating that Sn was not fully reacted with MgH_2. This phenomenon occurred due to the excessive catalyst amount.

Fig. 11 shows the comparison of the XRD patterns of the rehydrogenation between the $4MgH_2$–Sn (Fig. 11(a)) and $4MgH_2$–Sn-10 wt% TiF_3 (Fig. 11(b)) composites at 300 °C and under 33 atm of H_2 pressure. Only the Mg_2Sn peaks can be observed on the $4MgH_2$–Sn-10 wt% TiF_3 composites, and no peaks correspond to the MgH_2 Ti-containing and F-containing species. These results were similar to the MgH_2–Sn composite, where only the peaks of the Mg_2Sn could be observed, which suggested that the MgH_2–Sn destabilized system is not reversible. Even after the addition of TiF_3, the composite was still irreversible.

The results of this study showed that the formation of active species during the dehydrogenation process from the reaction of the MgH_2–Sn composite and 10 wt% TiF_3 cannot be detected by the XRD pattern due to its amorphous state or small amount. However, based on the XRD result for the sample mixing with 50 wt% TiF_3, it is proposed that the TiF_3 additive plays an important role in enhancing the dehydrogenation properties of the MgH_2–Sn composite via the in situ formation of an active species, namely MgF_2 and Ti. The catalytic effect of Ti-containing species and the active function of the F anion have been verified as important in enhancing the hydrogen sorption properties of metal/complex hydride [44–46]. The formation of Ti during the dehydrogenation process may play an important role in enhancement of the MgH_2–Sn composite because Ti is a good catalyst for MgH_2 [47,48]. In addition, Ma et al. [33] reported on the catalytic effects of TiF_3 in the decomposition of MgH_2, where the formation of MgF_2 plays a catalytic role, which leads to improved hydrogen storage performance. Therefore, TiF_3 additive plays a catalytic role in enhancing the hydrogen desorption temperature property of MgH_2–Sn by serving as the active site for nucleation and growth of dehydrogenation products. However, our efforts to make the MgH_2–Sn system reversible were unsuccessful due to the high equilibrium hydrogen pressures of the MgH_2–Sn composite.

4. Conclusions

TiF_3 plays a positive role in improving the hydrogen desorption properties of the MgH_2–Sn composite. From the TPD results, the onset temperature of hydrogen desorption of the $4MgH_2$–Sn-10 wt % TiF_3 involved two steps in the range of 140–160 °C and 250–270 °C. The MgH_2–Sn with the 4:1 mol ratio composite doped with 10 wt% of TiF_3 had a higher dehydrogenation rate at 150 °C compared to the as-received MgH_2, as-milled MgH_2 and $4MgH_2$–Sn with onset desorption temperatures at 434 °C, 355 °C and 250 °C, respectively. In addition, from the Kissinger plot, the activation energy of the first stage of the H-desorption of $4MgH_2$–Sn composite was reduced from 149.0 kJ/mol to 114.0 kJ/mol after the addition of 10 wt% TiF_3. These improvements were attributed to the formation of Ti-containing and F-containing catalytic species, which strengthen the interaction between MgH_2 and Sn and further enhance the dehydrogenation temperature of the composite. However, the addition of TiF_3 to the MgH_2–Sn composite did not result in improvement in the absorption measurement.

Acknowledgements

The authors would like to thank the Universiti Malaysia Terengganu for providing the facilities to run this project. This work was financially supported by Fundamental Research Grant Scheme (FRGS 59362). F. A. Halim Yap and N. N. Sulaiman acknowledges the Ministry of Education Malaysia for his MyBrain15 scholarship.

References

[1] E. David, An overview of advanced materials for hydrogen storage, J. Mater. Process. Technol. 162–163 (2005) 169–177.
[2] S. McWhorter, C. Read, G. Ordaz, N. Stetson, Materials-based hydrogen storage: attributes for near-term, early market PEM fuel cells, Curr. Opin. Solid State Mater. Sci. 15 (2011) 29–38.
[3] B. Sakintuna, F. Lamari-Darkrim, M. Hirscher, Metal hydride materials for solid hydrogen storage: a review, Int. J. Hydrogen Energy 32 (2007) 1121–1140.
[4] L. Li, C. An, Y. Wang, Y. Xu, F. Qiu, Y. Wang, L. Jiao, H. Yuan, Enhancement of the H_2 desorption properties of $LiAlH_4$ doping with $NiCo_2O_4$ nanorods, Int. J. Hydrogen Energy 39 (2014) 4414–4420.
[5] S. Huang, C. Liu, J. Li, P. Wang, H. Tian, First-principles study on the synergistic effects of Ti and F co-doping on the structure and dehydrogenation properties of $NaBH_4$, Int. J. Hydrogen Energy 39 (2014) 13512–13518.
[6] J. Wei, H. Leng, Q. Li, K.-C. Chou, Improved hydrogen storage properties of $LiBH_4$ doped Li-N-H system, Int. J. Hydrogen Energy 39 (2014) 13609–13615.
[7] M. Ismail, Y. Zhao, X.B. Yu, A. Ranjbar, S.X. Dou, Improved hydrogen desorption in lithium alanate by addition of SWCNT-metallic catalyst composite, Int. J. Hydrogen Energy 36 (2011) 3593–3599.
[8] B. Assfour, S. Leoni, G. Seifert, I.A. Baburin, Packings of carbon nanotubes-new materials for hydrogen storage, Adv. Mater 23 (2011) 1237–1241.
[9] M. Jorda-Beneyto, F. Suarez-Garcia, D. Lozano-Castello, D. Cazorla-Amoros, A. Linares-Solano, Hydrogen storage on chemically activated carbons and carbon nanomaterials at high pressures, Carbon 45 (2007) 293–303.
[10] M. Ismail, Y. Zhao, X.B. Yu, J.F. Mao, S.X. Dou, The hydrogen storage properties and reaction mechanism of the MgH_2–$NaAlH_4$ composite system, Int. J. Hydrogen Energy 36 (2011) 9045–9050.
[11] S. Milosevic, I. Milanovic, B.P. Mamula, A. Dukic, D. Rajnovic, L. Pasquini, J.G. Novakovic, Hydrogen desorption properties of MgH_2 catalysed with $NaNH_2$, Int. J. Hydrogen Energy 38 (2013) 12223–12229.
[12] J. Huot, G. Liang, S. Boily, A. Van Neste, R. Schulz, Structural study and hydrogen sorption kinetics of ball-milled magnesium hydride, J. Alloys Compd. 293–295 (1999) 495–500.
[13] A. Zaluska, L. Zaluski, J.O. Ström-Olsen, Nanocrystalline magnesium for hydrogen storage, J. Alloys Compd. 288 (1999) 217–225.
[14] A. Motavalli, M. Rajabi, Catalytic effect of melt-spun Ni_3FeMn alloy on hydrogen desorption properties of nanocrystalline MgH_2 synthesized by mechanical alloying, Int. J. Hydrogen Energy 39 (2014) 17047–17053.
[15] H. Leng, Y. Pan, Q. Li, K.-C. Chou, Effect of LiH on hydrogen storage property of MgH_2, Int. J. Hydrogen Energy 39 (2014) 13622–13627.
[16] M. Ismail, Influence of different amounts of $FeCl_3$ on decomposition and hydrogen sorption kinetics of MgH_2, Int. J. Hydrogen Energy 39 (2014) 2567–2574.
[17] M. Ismail, Effect of $LaCl_3$ addition on the hydrogen storage properties of MgH_2, Energy 79 (2015) 177–182.
[18] H. Liu, C. Wu, H. Zhou, T. Chen, Y. Liu, X. Wang, Z. Dong, H. Ge, S. Li, M. Yan, Synergistically thermodynamic and kinetic tailoring of the hydrogen desorption properties of MgH_2 by co-addition of AlH_3 and CeF_3, RSC Adv. 5 (2015) 22091–22096.
[19] A. Ranjbar, M. Ismail, Z.P. Guo, X.B. Yu, H.K. Liu, Effects of CNTs on the hydrogen storage properties of MgH_2 and MgH_2-BCC composite, Int. J. Hydrogen Energy 35 (2010) 7821–7826.
[20] A. Ranjbar, Z.P. Guo, X.B. Yu, D. Attard, A. Calka, H.K. Liu, Effects of SiC nanoparticles with and without Ni on the hydrogen storage properties of MgH_2, Int. J. Hydrogen Energy 34 (2009) 7263–7268.
[21] G.S. Walker, M. Abbas, D.M. Grant, C. Udeh, Destabilisation of magnesium hydride by germanium as a new potential multicomponent hydrogen storage system, Chem. Commun. 47 (2011) 8001–8003.
[22] M. Ismail, Y. Zhao, S.X. Dou, An investigation on the hydrogen storage properties and reaction mechanism of the destabilized MgH_2-Na_3AlH_6 (4:1) system, Int. J. Hydrogen Energy 38 (2013) 1478–1483.
[23] Y. Zhang, Q.-F. Tian, S.-S. Liu, L.-X. Sun, The destabilization mechanism and de/re-hydrogenation kinetics of MgH_2-$LiAlH_4$ hydrogen storage system, J. Power Sources 185 (2008) 1514–1518.
[24] H. Liu, X. Wang, Y. Liu, Z. Dong, G. Cao, S. Li, M. Yan, Improved hydrogen storage properties of MgH_2 by ball milling with AlH_3: preparations, de/rehydriding properties, and reaction mechanisms, J. Mater. Chem. A 1 (2013) 12527–12535.
[25] Y. Wang, Y. Wang, X. Wang, H. Zhang, L. Jiao, H. Yuan, Destabilization effects of $Mg(AlH_4)_2$ on MgH_2: improved desorption performances and its reaction mechanism, Int. J. Hydrogen Energy 39 (2014) 17747–17753.
[26] M. Ismail, Y. Zhao, X.B. Yu, S.X. Dou, Effect of different additives on the hydrogen storage properties of the MgH_2-$LiAlH_4$ destabilized system, RSC Adv. 1 (2011) 408–414.
[27] H. Liu, X. Wang, Y. Liu, Z. Dong, H. Ge, S. Li, M. Yan, Hydrogen desorption properties of the MgH_2-AlH_3 composites, J. Phys. Chem. C 118 (2014) 37–45.
[28] H.C. Zhong, H. Wang, L.Z. Ouyang, M. Zhu, Microstructure and hydrogen storage properties of Mg-Sn nanocomposite by mechanical milling, J. Alloys Compd. 509 (2011) 4268–4272.
[29] G. Urretavizcaya, G.O. Meyer, Metastable hexagonal Mg_2Sn obtained by mechanical alloying, J. Alloys Compd. 339 (2002) 211–215.
[30] H. Imamura, K. Yoshihara, M. Yoo, I. Kitazawa, Y. Sakata, S. Ooshima, Dehydriding of Sn/MgH_2 nanocomposite formed by ball milling of MgH_2 with Sn, Int. J. Hydrogen Energy 32 (2007) 4191–4194.
[31] H. Imamura, K. Tanaka, I. Kitazawa, T. Sumi, Y. Sakata, N. Nakayama, S. Ooshima, Hydrogen storage properties of nanocrystalline MgH_2 and MgH_2/Sn nanocomposite synthesized by ball milling, J. Alloys Compd. 484 (2009) 939–942.
[32] M. Ismail, Y. Zhao, X.B. Yu, S.X. Dou, Improved hydrogen storage performance of MgH_2–$NaAlH_4$ composite by addition of TiF_3, Int. J. Hydrogen Energy 37 (2012) 8395–8401.
[33] L.-P. Ma, P. Wang, H.-M. Cheng, Improving hydrogen sorption kinetics of MgH_2 by mechanical milling with TiF_3, J. Alloys Compd. 432 (2007) L1–L4.
[34] R.A. Varin, M. Jang, T. Czujko, Z.S. Wronski, The effect of ball milling under hydrogen and argon on the desorption properties of MgH_2 covered with a layer of $Mg(OH)_2$, J. Alloys Compd. 493 (2010) L29–L32.
[35] M. Ismail, Y. Zhao, X.B. Yu, I.P. Nevirkovets, S.X. Dou, Significantly improved dehydrogenation of $LiAlH_4$ catalysed with TiO_2 nanopowder, Int. J. Hydrogen Energy 36 (2011) 8327–8334.
[36] M. Ismail, Y. Zhao, X.B. Yu, S.X. Dou, Improved hydrogen storage property of $LiAlH_4$ by milling with carbon based additives, Int. J. Electroact. Mater. 1 (2013) 13–22.
[37] M. Ismail, A. Sinin, C. Sheng, W.W. Nik, Desorption behaviours of lithium alanate with metal oxide nanopowder additives, Int. J. Electrochem. Sci. 9 (2014) 4959–4973.
[38] M. Ismail, Y. Zhao, X.B. Yu, S.X. Dou, Effects of NbF_5 addition on the hydrogen storage properties of $LiAlH_4$, Int. J. Hydrogen Energy 35 (2010) 2361–2367.
[39] H.E. Kissinger, Reaction kinetics in differential thermal analysis, Anal. Chem. 29 (1957) 1702–1706.
[40] N.S. Mustafa, M. Ismail, Influence of K_2TiF_6 additive on the hydrogen sorption properties of MgH_2, Int. J. Hydrogen Energy 39 (2014) 15563–15569.
[41] F.A. Halim Yap, N.S. Mustafa, M. Ismail, A study on the effects of K_2ZrF_6 as an additive on the microstructure and hydrogen storage properties of MgH_2, RSC Adv. 5 (2015) 9255–9260.
[42] G. Liang, Synthesis and hydrogen storage properties of Mg-based alloys, J. Alloys Compd. 370 (2004) 123–128.
[43] J. Mao, Z. Guo, X. Yu, M. Ismail, H. Liu, Enhanced hydrogen storage performance of $LiAlH_4$-MgH_2-TiF_3 composite, Int. J. Hydrogen Energy 36 (2011) 5369–5374.
[44] L.P. Ma, X.D. Kang, H.B. Dai, Y. Liang, Z.Z. Fang, P.J. Wang, P. Wang, H.M. Cheng, Superior catalytic effect of TiF_3 over $TiCl_3$ in improving the hydrogen sorption kinetics of MgH_2: catalytic role of fluorine anion, Acta Mater. 57 (2009) 2250–2258.
[45] N.S. Mustafa, N.H. Idris, M. Ismail, Effect of K_2TiF_6 additive on the hydrogen storage properties of $4MgH_2$–$LiAlH_4$ destabilized system, Int. J. Hydrogen Energy 40 (2015) 7671–7677.
[46] N. Juahir, N.S. Mustafa, F.A. Halim Yap, M. Ismail, Study on the hydrogen storage properties and reaction mechanism of $NaAlH_4$–$Mg(BH_4)_2$ (2:1) with and without TiF_3 additive, Int. J. Hydrogen Energy 40 (2015) 7628–7635.
[47] R.R. Shahi, A.P. Tiwari, M.A. Shaz, O.N. Srivastava, Studies on de/rehydrogenation characteristics of nanocrystalline MgH_2 co-catalyzed with Ti, Fe and Ni, Int. J. Hydrogen Energy 38 (2013) 2778–2784.
[48] C.X. Shang, M. Bououdina, Y. Song, Z.X. Guo, Mechanical alloying and electronic simulations of (MgH_2+M) systems (M=Al, Ti, Fe, Ni, Cu and Nb) for hydrogen storage, Int. J. Hydrogen Energy 29 (2004) 73–80.